Biosensors and Bioelectronics 296 (2026) 118312

Contents lists available at ScienceDirect

Biosensors and Bioelectronics

journal homepage: www.elsevier.com/locate/bios

# A daily-durable wearable sweat biosensing device with robust reticular conductive biogel interface

Qian Yu [a], Jun Sun [a], Chen Yuan [a], Chao Zhao [b], Yunlong Chen [a], Jie Wu [a,*], Siqi Yu [a], Hong Liu [b], Huangxian Ju [a,**]

[a] State Key Laboratory of Analytical Chemistry for Life Science, School of Chemistry and Chemical Engineering, Nanjing University, Nanjing, 210023, PR China
[b] State Key Laboratory of Digital Medical Engineering, Southeast University, Nanjing, 211189, PR China

ARTICLE INFO

*Keywords:*
Wearable sensors
Metal-organic frameworks
Conductive hydrogel
Electrochemical biosensor
Durability
Sweat analysis

ABSTRACT

Wearable biosensing devices are essential for managing chronic diseases at home. However, their clinical translation has been hindered by the poor durability and stability of biosensors during long-term use in real-world scenarios. Here, we report a daily-durable wearable electrochemical biosensor array by encapsulating ZIF-90@enzymes within a conductive gel matrix to form a robust reticular biogel interface for continuous analysis of sweat glucose and lactate. The wearable biosensors exhibit exceptional environmental adaptability and durability, retaining >95 % sensitivity after summer outdoor exposure for 10 h and >85 % sensitivity after 1000 bends. In addition, they also demonstrate excellent pH and temperature tolerance, and the room-temperature storage stability of 140 days. By integrating the biosensor array with a paper-based sweat collector and a printed circuit board, the proposed wearable device enables on-body sweat analysis during both vigorous exercise (e.g., running) and daily activities, showing its application prospects in routine health monitoring.

## 1. Introduction

Wearable biosensors are highly integrated analytical devices that can be directly worn on the skin of different body parts or embedded into daily accessories (Lin et al., 2021; Rwei et al., 2020). They enable long-term, real-time, and continuous monitoring of biochemical parameters through minimally invasive or non-invasive methods, thereby facilitating health monitoring at the molecular level and improving chronic disease management (Sempionatto et al., 2022; Madhvapathy et al., 2025). Various wearable biosensors have been developed for detecting the targets in different biological fluids, including urine, saliva, tears, sweat, and even interstitial fluid (Brasier et al., 2024). Among them, sweat biosensors are the most prominent, as sweat contains rich biomolecules relevant to physiological health and has been clinically validated for diagnostics, for instance, in cystic fibrosis diagnosis (Ray et al., 2021). In addition, unlike tear, which must be collected near the eyes, sweat can be conveniently sampled from any region of the body due to the ubiquitous distribution of sweat glands (Yang et al., 2023).

Wearable sweat biosensors have undergone rapid development in recent years. For example, through user-friendly all-in-one designs (Baik et al., 2021), sweat biosensors achieve at-home monitoring and remote diagnosis, advancing intelligent personalized healthcare management. Furthermore, by developing highly stretchable and biocompatible flexible sensing materials (Gong et al., 2024) with bioinspired nanoarchitectures and biomimetic skin-like structures, and incorporating self-powering systems such as solar cells (Min et al., 2023), biofuel cells (Bandodkar et al., 2020), and triboelectric generators (Dong et al., 2020), these sensors have achieved significant improvements in durability, wear comfort, and practical applicability. Currently, various wearable sweat sensing devices have been proposed for on-body monitoring of biomolecules including glucose (Bai et al., 2024; Ding et al., 2024), lactic acid (Arwani et al., 2024; Ding et al., 2024), uric acid (Yang et al., 2020), nutrients (Yang et al., 2020; Wang et al., 2022), cortisol (Parlak et al., 2018; Torrente-Rodriguez et al., 2020) and cytokines (Jagannath et al., 2021). These devices have successfully demonstrated proof-of-concept applications in multiple fields, including diabetes management (Gao et al., 2016; Arwani et al., 2024), athlete training

* Corresponding author.
** Corresponding author.
*E-mail addresses:* wujie@nju.edu.cn (J. Wu), hxju@nju.edu.cn (H. Ju).

https://doi.org/10.1016/j.bios.2025.118312
Received 16 September 2025; Received in revised form 27 November 2025; Accepted 12 December 2025
Available online 13 December 2025

intensity and endurance evaluation (Gao et al., 2016; Xu et al., 2023), gout and kidney disease monitoring (Kim et al., 2020; Chen et al., 2023), immunoassay (Wang et al., 2022), and medication guidance for Parkinson's disease treatment. However, their clinical translation still faces numerous challenges (Davis et al., 2024). Particularly, for outdoor applications, the biosensors must maintain high robustness, stability, and reliability under diverse environmental conditions encountered in daily life.

To enhance the environmental robustness of wearable biosensors and eliminate the motion artifacts caused by skin-device friction, numerous advanced materials featuring high biocompatibility, ultra-compliance, and excellent skin conformability have been developed (Yin et al., 2022, 2024; Wang et al., 2025). However, prolonged solar radiation compromises wearable electrochemical sensors through two primary pathways: localized heating that distorts measurements, and photo-degradation that undermines the integrity of polymers, mediators, and sensing elements. Solar radiation compromises wearable biosensors by degrading their constituent materials (e.g., polymers) (Hardy et al., 2022; Semperger et al., 2022; Petroody et al., 2023), which impairs electrical conductivity and mechanical stability, thereby reducing device lifespan. However, mitigation strategies for this interference mechanism remain underdeveloped, hindering widespread outdoor deployment. Beyond solar radiation, the practical performance of wearable biosensors depends critically on storage stability and resilience to environmental stresses such as temperature fluctuations, and mechanical strain. Addressing these challenges is essential for ensuring their long-term reliability and successful real-world deployment. Metal-organic frameworks (MOFs), a class of porous crystalline materials, have shown exceptional promise for enzyme stabilization (Furukawa et al., 2013; Liang et al., 2015, 2019; Li et al., 2022) owing to their high surface area, tunable porosity, excellent thermal stability and inherent biocompatibility (Shieh et al., 2015; Mohan et al., 2024; Sun et al., 2025), which endow MOF@enzyme composites with substantial potential for developing robust wearable biosensors, even for outdoor applications. However, the development of MOF-based wearable electrochemical sensors is hindered by the inherent trade-off between enhancing conductivity, typically through the incorporation of secondary materials (Yao et al., 2017; Yang et al., 2022; Su et al., 2023), and preserving critical properties such as high porosity and stable adhesion. Achieving a seamless integration of high conductivity, preserved porosity, and robust adhesion into a single, functional platform remains a major challenge.

In this work, we fabricated a daily-durable wearable electrochemical biosensor array by in situ forming robust reticular conductive biosensing gel interfaces on screen-printed carbon electrodes (SPCEs) with sensing membrane cocktails, which were prepared by dispersing enzyme-encapsulated zeolitic imidazolate frameworks (ZIF-90@enzymes) in gel pre-reaction solutions, and then mixing the dispersions with electron mediators, respectively. The gel pre-reaction solutions contained poly (3,4-ethylenedioxythiophene): poly(styrenesulfonate) (PEDOT: PSS) for achieving high conductivity of the gel interfaces, and acrylamide for forming a gel matrix with N, N′-methylenebisacrylamide (MBA). Using glucose oxidase (GOx) and lactate dehydrogenase (LDH) for the synthesis of ZIF-90@enzymes, the prepared wearable glucose and lactate sensors array exhibited exceptional environmental durability along with more than 95 %, 92 % and 85 % of initial detection sensitivity after outdoor exposure to solar radiation for 10 h, consecutive testing for 28 cycles, and 1000 bending-recovery cycles, respectively. In addition, the biosensors showed good acid tolerance across a wide pH range of 4–8 and long-term storage stability up to 140 days at room temperature. On-body test of the integrated wearable biosensing device also demonstrated its robustness for prolonged, continuous monitoring of sweat glucose and lactate during both outdoor running trials and indoor thermal stimulation experiments, indicating the practicality in daily personalized healthcare management.

## 2. Experimental section

### 2.1. Preparation of a SPCE-based biosensor array

The biosensor array was constructed on a flexible SPCE (Eaglenos Sciences, Inc., China), which consisted of a carbon counter electrode, a Ag/AgCl reference electrode, and two carbon WEs ($WE_1$ and $WE_2$) for the preparation of glucose and lactate sensors, respectively.

Synthesis of ZIF-90@enzymes: ZIF-90@GOx and ZIF-90@LDH were synthesized using a de novo approach (Shieh et al., 2015). Firstly, 371.25 mg of imidazole-2-carboxaldehyde, 50 mg of polyvinylpyrrolidone, and 25 mg of GOx (or LDH) were dissolved in 25 mL of deionized water. Then, 3 mL of 0.653 M $Zn(NO_3)_2$ solution was quickly added under stirring, and the mixture was allowed to react for 30 min at room temperature to obtain ZIF-90@GOx (or ZIF-90@LDH). After washing with deionized water for 6 times, the resulting ZIF-90@GOx and ZIF-90@LDH were dispersed in 8.75 mL of gel pre-reaction solution 1 and 2, respectively. Here, gel pre-reaction solution 1 contained 0.067 wt% of PEDOT: PSS, 0.5 M of acrylamide, and 0.2 M of MBA, while gel pre-reaction solution 2 contained 0.067 wt% of PEDOT:PSS, 0.5 M of acrylamide, 0.02 M of AAPBA, and 0.2 M of MBA. The obtained dispersions of ZIF-90@enzymes were stored at 4 °C for further use.

Preparation of glucose sensor: Firstly, 35 μL of ZIF-90@GOx dispersion, 3 μL of 43.8 mg $mL^{-1}$ PBNPs (Yu et al., 2025), and 65 μL of gel pre-reaction solution 1 were mixed to prepare the glucose sensing membrane cocktail. Then, 4 μL of the cocktail and 1 μL of catalyst solution were sequentially dropped on $WE_1$, followed by drying in a desiccator to obtain the glucose sensor. Here, the catalyst solution was prepared by mixing 0.02 M ammonium persulfate ($(NH_4)_2S_2O_8$) with N, N, N′, N′-tetramethylethylenediamine (TEMED, ≥99 %) in a volume ratio of 9:1.

Preparation of lactate sensor: After 40 mg of $NAD^+$ was dissolved in 1 mL of gel pre-reaction solution 2, 30 μL of the solution was mixed with 70 μL of ZIF-90@LDH dispersion and 3 μL of 600 mg $mL^{-1}$ hematin to prepare the lactate sensing membrane cocktail. 4 μL of the cocktail and 1 μL of catalyst solution were sequentially dropped on $WE_2$ to dry in a desiccator for obtaining the lactate sensor.

### 2.2. Preparation of paper-based sweat collector

The paper-based sweat collector was fabricated by $CO_2$ laser engraving (Optima-5070, Nanjing Chaohan Digital Machinery, China) on a Whatman qualitative filter paper (Yu et al., 2025). Its pattern was designed using Laser Work v.6 software to include a central square sweat collection zone (4 × 4 $mm^2$), surrounded by 4 capillary input channels (9 mm × 0.6 mm each), each with 3 circular inlets (2 mm in diameter), and 1 outlet channel (18 mm × 1.6 mm) connecting to a waste zone (25.9 × 38.6 $mm^2$).

### 2.3. Fabrication of a wearable biosensing device

The wearable biosensing device was fabricated by interfacing a PCB (Yu et al., 2025) with a wearable patch. The wearable patch was assembled sequentially by an inlet layer, a SPCE-based biosensor array, and the paper-based sweat collector containing a sweat collection zone and a waste zone separated by a sealing layer. Here, the inlet layer and sealing layer were made of commercial double-sided medical adhesive tape (thickness <50 μm). The inlet layer was fabricated via $CO_2$ laser engraving to create inlet holes, which precisely aligned with the inlet pattern of the sweat collector. During the assembly, the collection zone and the inlets of the sweat collector were stacked onto the biosensor array and the corresponding inlet holes, respectively, followed by enclosing with the sealing layer. Finally, the waste zone of the paper-based sweat collector was folded over the sealing layer, forming the wearable patch.

The current design employed a rigid PCB to host the core electronics

(microcontroller and wireless module), yet its inherent rigidity compromised the comfort of the flexible sensing patch. Future iterations should transition to flexible printed circuits (FPC) or rigid-flex designs to resolve this mechanical mismatch.

### 2.4. Human experiment

Human subject recruitment: All human experiments were conducted under a protocol approved by the Medical Ethics Subcommittee of Science and Technology Ethics Committee of Nanjing University (No. OAP2023082001), in compliance with relevant laws and ethical regulations. 12 healthy volunteers (6 males and 6 females, aged 18–30 years) were recruited from the campus of Nanjing University through advertisements. Written informed consents were obtained from all participants before they participated in the study.

On-body testing of wearable sweat biosensing device: One hour after eating, volunteers were asked to wear the wearable device and perform a 60-min stationary running exercise at a speed of 6 km $h^{-1}$ (SH-5199, SHUA Sports) in a ventilated indoor environment with a humidity of 50–60 % at 25 °C. During the on-body trial, data were recorded by the

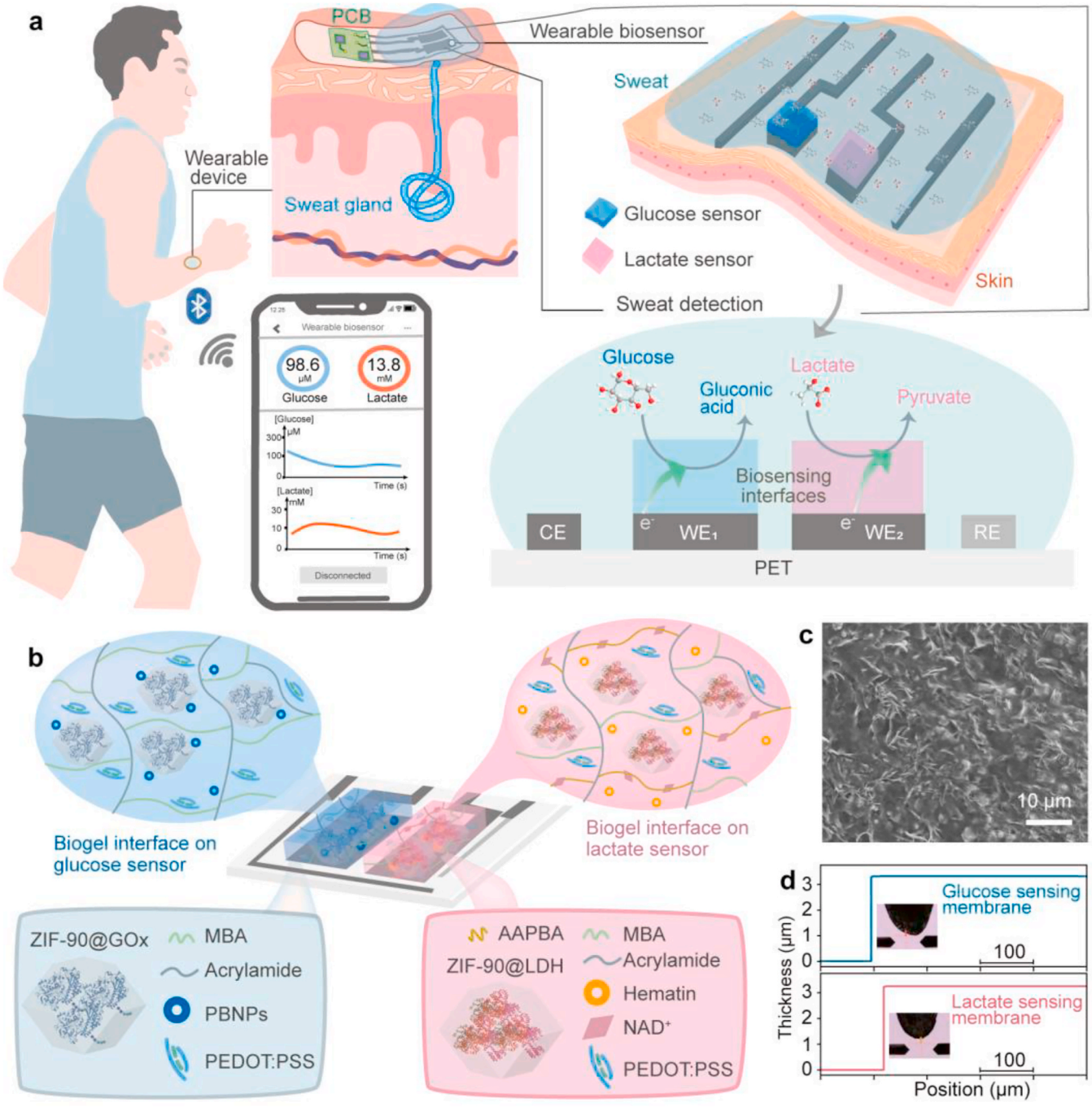


**Fig. 1.** Design schematic of biosensors-integrated wearable device. (a) Schematic of wearable biosensors for on-skin monitoring of sweat glucose and lactate with data display on a mobile phone via Bluetooth. CE, counter electrode; RE, reference electrode; $WE_1$, working electrode 1; $WE_2$, working electrode 2; PET, polyethylene terephthalate; PCB, printed circuit board. (b) Schematic diagram of reticular conductive biogel interfaces on glucose and lactate sensors. PBNPs, Prussian blue nanoparticles. AAPBA, 3-acrylamidophenylboronic acid. (c) SEM image of reticular conductive biogel interface on lactate sensor. (d) Step profile of the sensing membranes on SPCEs. (For interpretation of the references to color in this figure legend, the reader is referred to the Web version of this article.)

PCB and wirelessly transmitted to a mobile phone via Bluetooth. The detection of glucose and lactate was performed at 10 min after starting exercise and repeated every 10 min until the exercise concluded. The concentrations of glucose and lactate were visualized on a custom smartphone application through calculation based on pre-established calibration curves. Meanwhile, sweat samples were periodically collected from the forearms of participants using centrifuge tubes and analyzed using a glucose colorimetric assay kit and lactate assay kit with WST-8 (Beyotime Biotechnology, China) to validate the detection accuracy of the proposed wearable sweat biosensing device. In addition, 2 volunteers wearing the wearable device were asked to monitor sweat glucose and lactate levels for 12 cycles of 20-min thermal stimulation from heating pads to sweat and 40-min intervals accompanied by non-exercise daily activities such as food intake, standing, and sitting. It was also important to note that during high-intensity exercise movement of the rigid PCB and poor skin contact caused occasional signal instability.

Synchronous blood analysis: To synchronize with the sweat

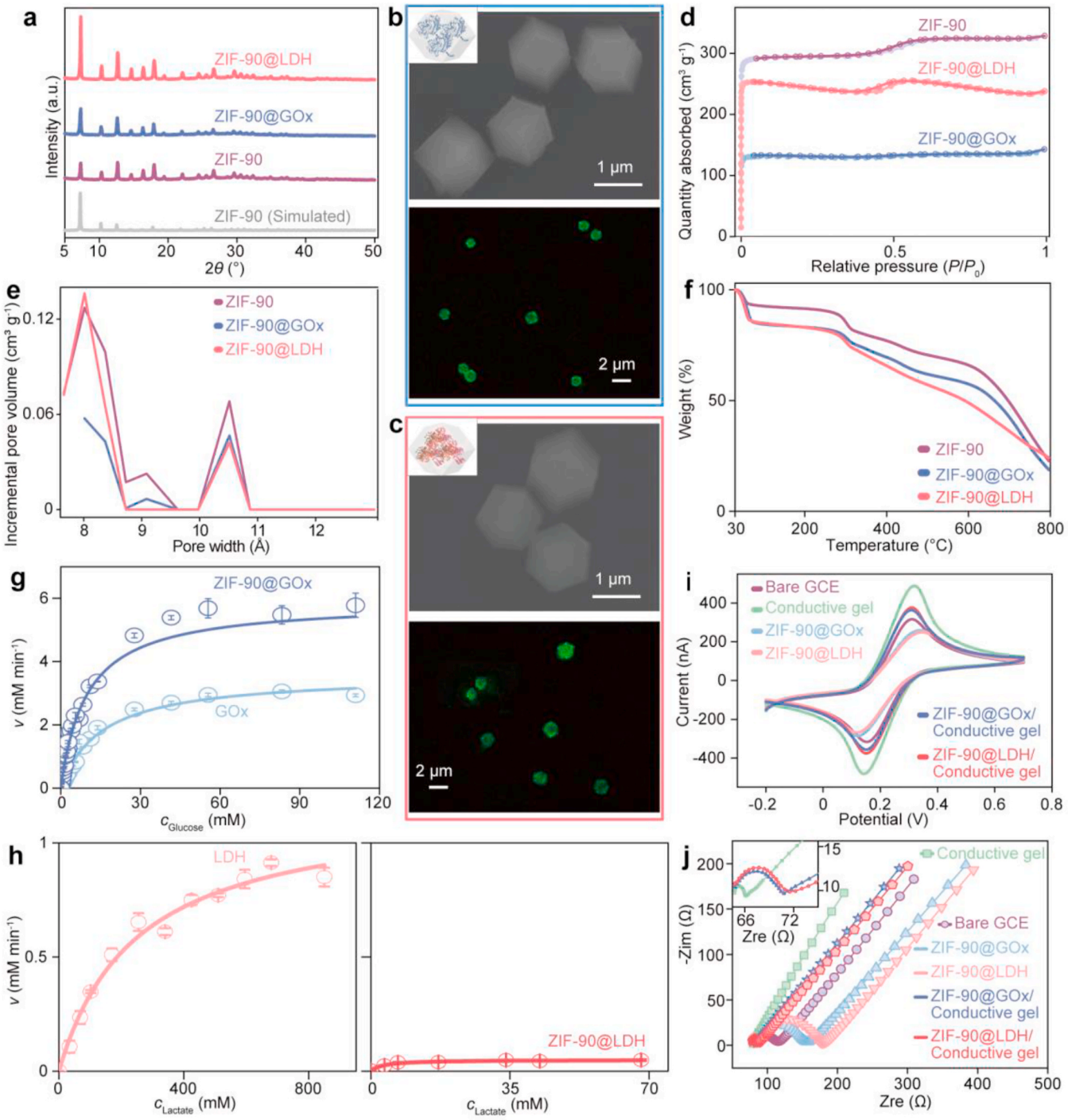


**Fig. 2.** Characterization of reticular conductive biogel interfaces. (a) XRD patterns of ZIF-90 and ZIF-90@enzymes. (b, c) SEM and confocal microscopic images of ZIF-90@GOx (b) and ZIF-90@LDH (c). (d–f) $N_2$ adsorption-desorption isotherms (d), pore size distributions (e), and TGA curves (f) of ZIF-90 and ZIF-90@enzymes. (g, h) Enzyme kinetic curves of GOx, ZIF-90@GOx (g), LDH and ZIF-90@LDH (h). Data are presented as mean ± SD, $n = 3$. (i, j) CV curves (i) and EIS spectra (j) of different modified electrodes.

measurements during running exercise, glucose and lactate levels in fingertip capillary blood were measured at 10-min intervals. Blood samples were collected using a fingerprick approach (Yu et al., 2025). Blood glucose concentrations were measured using a commercial glucometer (Bayer), while lactate concentrations were determined using a lactate assay kit (Nanjing Jiancheng Bioengineering Institute, China).

## 3. Results and discussion

### 3.1. Overview of the wearable sweat biosensing device

The wearable sweat biosensing device featuring a dual-sensor array was constructed on a two-channel flexible SPCE. The array was interfaced with a printed circuit board (PCB) and attached to any region of body, such as forearm, for real-time on-body detection of sweat glucose and lactate levels, with the data wirelessly transmitted and displayed on a mobile device via Bluetooth (Fig. 1a, and Video S1). The wearable biosensors were prepared by drop-coating the glucose and lactate sensing membrane cocktails and catalyst solution on screen-printed carbon working electrodes 1 and 2 ($WE_1$ and $WE_2$) to form reticular conductive biogel membranes, respectively (Fig. 1b and c). The cocktails contained ZIF-90@enzymes and Prussian blue nanoparticles (PBNPs) or nicotinamide adenine dinucleotide ($NAD^+$) and hematin as the electron mediators for glucose or lactate biosensing. The membrane thickness was measured to be 3.3 μm (Fig. 1d).

Supplementary video related to this article can be found at https://doi.org/10.1016/j.bios.2025.118312

### 3.2. Characterization of ZIF-90@enzymes and biosensing gel interface

ZIF-90@enzymes were synthesized by a one-pot preparation method (Shieh et al., 2015). Both.

ZIF-90@GOx and ZIF-90@LDH displayed identical X-ray powder diffraction (XRD) patterns to pure ZIF-90 (Fig. 2a), indicating that ZIF-90@enzymes retained the crystalline reticular structure of ZIF-90. They also exhibited a rhombic dodecahedron structure with an approximate size of 1 μm (Fig. 2b and c). The loadings of GOx and LDH were measured to be $4.88 \times 10^6$ and $5.30 \times 10^6$ per particle, respectively (Fig. S1). The Brunauer-Emmett-Teller (BET) surface area and pore volume were 396.43 $m^2\ g^{-1}$ and 0.22 $cm^3\ g^{-1}$ for ZIF-90@GOx, and 733.08 $m^2\ g^{-1}$ and 0.37 $cm^3\ g^{-1}$ for ZIF-90@LDH, which were significantly lower than 930.05 $m^2\ g^{-1}$ and 0.51 $cm^3\ g^{-1}$ of ZIF-90 (Fig. 2d, and S2), indicating successful enzyme encapsulation within ZIF-90 pores. The pore size distribution of ZIF-90@enzymes was similar to that of ZIF-90 (Fig. 2e), further confirming the retention of the reticular structure and uniform enzyme encapsulation within ZIF-90. Thermogravimetric (TGA) analysis revealed that both ZIF-90@GOx and ZIF-90@LDH exhibited similar mass loss profiles to ZIF-90 across the decomposition temperature range, suggesting that the enzyme encapsulation did not compromise the thermal stability of ZIF-90 (Fig. 2f).

The specific enzyme activities (SAs) of ZIF-90@GOx and ZIF-90@LDH were measured using UV–visible absorption spectrometry to be 145 and 17 U $mg^{-1}$, respectively, which were lower than those of free GOx (216 U $mg^{-1}$) and LDH (38 U $mg^{-1}$) due to partial inaccessibility or structural perturbation of active sites upon encapsulation (Fig. S3–S4). However, their Michaelis constants ($K_m$) were significantly reduced to 9.9 and 0.73 mM from 15 to 24 mM of free GOx and LDH, respectively (Fig. 2g and h). The $k_{cat}/K_m$ values for ZIF-90@GOx and ZIF-90@LDH were calculated as 62.6 and 11.7 $mM^{-1}\ s^{-1}$, respectively, exceeding both 49.6 and 0.75 of free enzymes (Table S1). These results suggest that the encapsulation of enzymes within the ZIF-90 framework improved both the substrate affinity and the catalytic kinetics of enzymes. The incorporation of the conductive gel significantly enhanced the electron-transfer kinetics of both ZIF-90@GOx and ZIF-90@LDH-modified electrodes. The ZIF-90@GOx/conductive gel and ZIF-90@LDH/conductive gel electrodes exhibited peak current increases by 40.8 % and 51.3 %, respectively (Fig. 2i). Correspondingly, their charge-transfer resistance ($R_{ct}$) decreased dramatically from 92.8 to 10.9 Ω and 114.5 to 12.4 Ω, respectively (Fig. 2j and Table S2). This kinetic enhancement was quantified by the electron transfer rate constant ($k_0$), which increased to $2.3 \times 10^{-3}$ and $2.2 \times 10^{-3}$ cm $s^{-1}$, respectively, representing 11.5-fold and 13.8-fold improvements over their counterparts without conductive gel (Table S2). Thus, the conductive gel was proven to be pivotal in facilitating interfacial electron transfer.

### 3.3. Characterization of glucose sensor

The glucose sensor employed ZIF-90@GOx to catalyze the oxidation of glucose by dissolved oxygen to produce $H_2O_2$, while PBNPs served as an electron mediator of $H_2O_2$ oxidation to generate the electrochemical signal (Fig. 3a). The electronegative environment introduced by imidazole-2-carboxaldehyde (ICA) ligands in the ZIF-90 framework facilitated electron migration from $Fe^{2+}$ to.

OOH across the cyanide bridge (-C ≡ N-Fe-), which enhanced the Fe-O stretching of Fe-OH and Fe-OOH at 573 and 690 $cm^{-1}$ (Fig. S5), thereby promoting the electron transfer from electrode to $Fe^{3+}$ (Fig. 3b). Consequently, the glucose sensor utilizing this mechanism achieved a high detection sensitivity of 93 ± 3 nA $cm^{-2}$ $\mu M^{-1}$ over a glucose concentration range of 0–300 μM (Fig. 3c, and S6, and Table S3). Moreover, the cyclic detection performance was also excellent, which showed a sensitivity variation of 8 % over 28 consecutive cycles of standard curve testing (Fig. 3d, and S7). This glucose sensor showed good selectivity and fabrication reproducibility, with relative standard deviations (RSD) of 2.8 % for within-batch sensors and 5.1 % for between-batch sensors (Figs. S8–S9, and Table S4). Additionally, it demonstrated reversible performance (Fig. 3e). The excellent stability of the glucose sensor was demonstrated by both 91 % of its initial response over an 8-h continuous monitoring in a flow-sampling model (Fig. 3f) and almost constant detection sensitivity and current density after storage for 140 days at room temperature (Fig. 3g and S10), which exhibited better storage stability compared to recently reported wearable glucose sensors (Fig. 3h, and Table S3), highlighting its superior performance in practical applications. Especially, the proposed sensor showed stable detection sensitivity across a pH range of 4.0–8.0 and a temperature range of 20–50 °C (Fig. 3i, j, and S11), benefiting from the protective effect of the ZIF-90 reticular structure on GOx. These results demonstrated good environmental robustness of the glucose sensor, which enabled its routine applications without the need for frequent pH and temperature calibration.

### 3.4. Characterization of lactate sensor

The lactate sensor was performed using ZIF-90@LDH to catalyze the oxidation of lactate in the presence of $NAD^+$, and the resulting NADH was then electrochemically oxidized at −0.0 V (vs. Ag/AgCl) with hematin as an electron mediator to produce the amperometric response (Fig. 4a and S12). It showed a linear response to lactate ranging from 0 to 30 mM, with a detection sensitivity of 874 ± 34 nA $mM^{-1}$ $cm^{-2}$ (Fig. 4b). Similarly, the lactate sensor also exhibited good selectivity and fabrication reproducibility, with RSD of 4.0 % for within-batch sensors and 2.6 % for between-batch sensors (Figs. S13–S14, and Table S4). The sensitivity over multiple testing cycles showed only 7 % variation (Fig. 4c and S15), and the cyclic detection also showed good reversibility (Fig. 4d). The proposed sensor demonstrated reliable continuous monitoring performance, which maintained 93 % of its initial current response over lactate detection for 4 h under a flow-sampling model (Fig. 4e). Notably, the sensor retained approximately 93 % of its initial sensitivity and response signal even after storage for 170 days at room temperature (Fig. 4f and S16), demonstrating the much better storage stability than those of previously reported lactate sensors (Gao et al., 2016; Istrate et al., 2021; Schuck et al., 2021; Thapa et al., 2021;

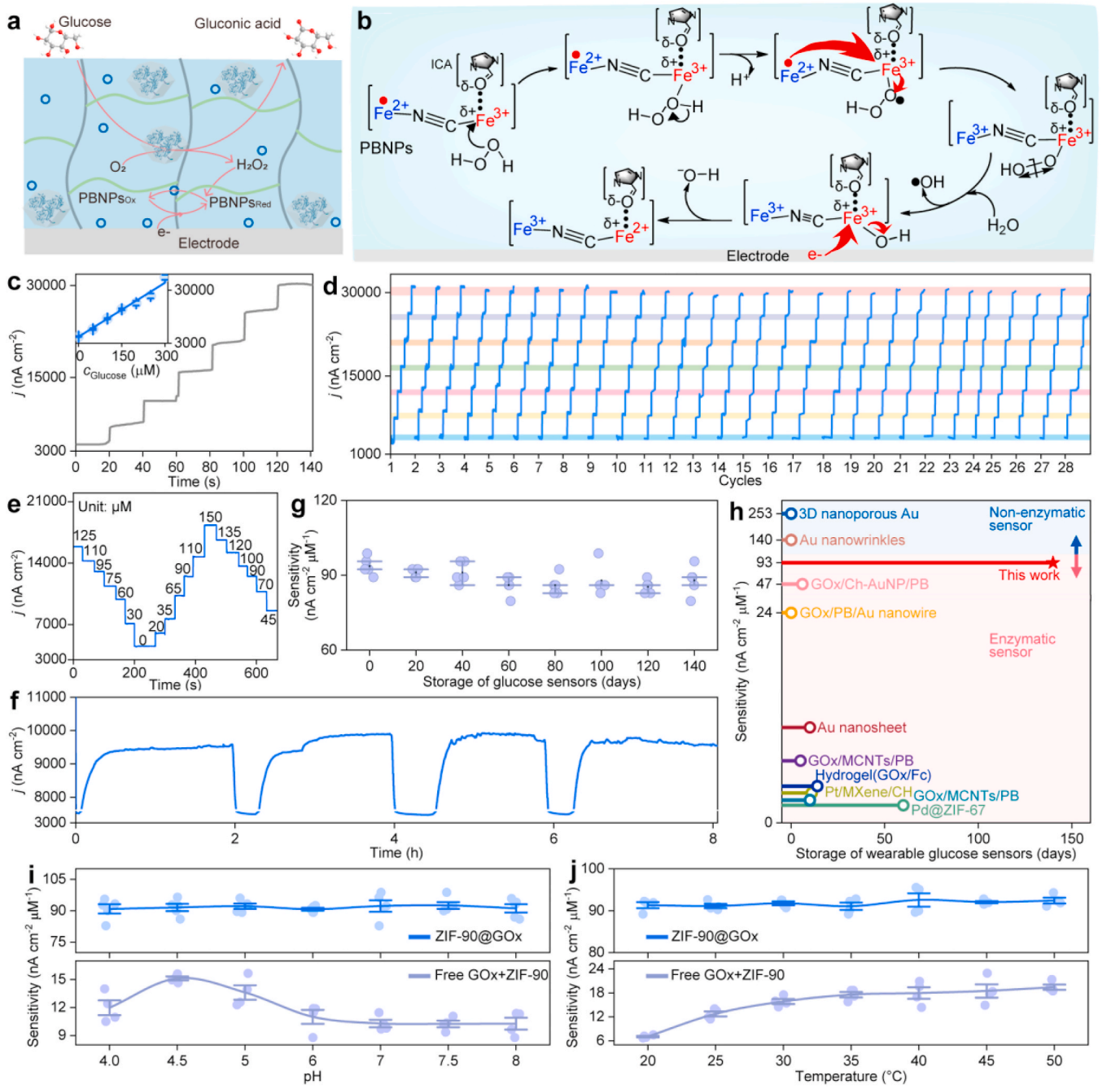


**Fig. 3.** Characterization of glucose sensor. (a) Diagram of glucose-sensing mechanism. (b) Reaction mechanism in the reticular gel during glucose sensing. (c) Amperometric responses of the glucose sensor at 0.0 V upon glucose additions. Inset: calibration curve. Data are presented as mean ± SD, $n = 6$. (d) Continuous testing upon 6 additions of 50 μM glucose for 28 cycles with a single glucose sensor. (e) Reversible response to varying glucose concentrations. (f) Continuous detection of 100 μM glucose under flow-injection conditions. (g) Detection sensitivities of glucose sensors during 140-day storage. Data are presented as mean ± SD, $n = 4$. (h) Storage stability comparison of wearable glucose sensors prepared with different materials. (i, j) Effects of pH (i) and temperature (j) on the sensitivity of glucose sensors prepared with GOx or ZIF-90@GOx. Data are presented as mean ± SD, n = 4.

Komkova et al., 2022; Saha et al., 2022; Kumar et al., 2023; Xuan et al., 2023; Li et al., 2024; Weng et al., 2024; Wu et al., 2024) (Fig. 4g). Owing to the protective effect of the ZIF-90 reticular structure, the lactate sensor showed stable detection sensitivity against pH change from 4.0 to 8.0 (Fig. 4h and S17a), and its ability against temperature change was also enhanced (Fig. 4i and S17b). Unfortunately, the detection sensitivity slightly increased with the increasing temperature from 20 to 45 °C, but could be automatically calibrated for routine applications due to the linear change.

### 3.5. *Performance of wearable biosensing device*

A systematic comparison of individual components confirmed the robustness of our reticular conductive biogel interface (Figs. S6 and S18-S19) and elucidated the "dual-stage stabilization mechanism". Firstly, incorporating the plain gel (without PEDOT:PSS) improved the response time and signal stability during the successive addition of 50 μM glucose or 5 mM lactate, compared to the enzyme-only electrode, although it did not enhance sensitivity. This is attributed to the gel's hydrated microenvironment and interface stabilization. Furthermore, replacing the

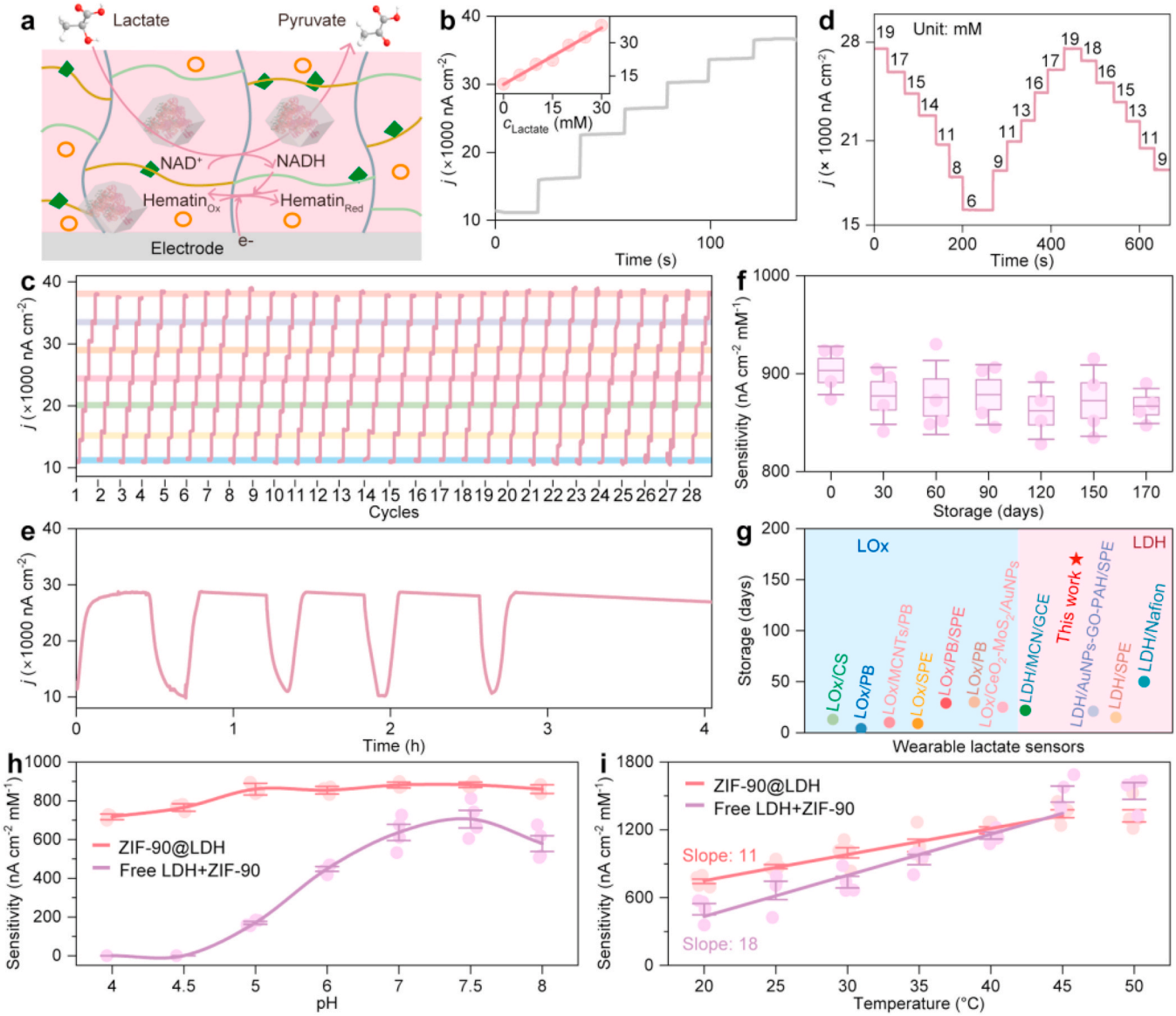


**Fig. 4.** Characterization of lactate sensor. (a) Diagram of lactate-sensing mechanism. (b) Amperometric responses of the lactate sensor at 0.0 V upon lactate additions. Inset: calibration curve. Data are presented as mean ± SD, $n = 6$. (c) Continuous testing upon 6 additions of 5 mM lactate for 28 cycles with a single lactate sensor. (d) Reversible detection at varying lactate concentrations. (e) Continuous response to 20 mM lactate under flow-injection conditions. (f) Detection sensitivities of lactate sensors during 170-day storage. Data are presented as mean ± SD, $n = 4$. (g) Storage stability comparison of wearable lactate sensors prepared with different materials. (h, i) Effects of pH (h) and temperature (i) on the sensitivity of lactate sensors prepared with LDH or ZIF-90@LDH. Data are presented as mean ± SD, $n = 3$.

plain gel with the conductive gel resulted in a significant sensitivity enhancement, 2.3-fold and 3.8-fold for the GOx and LDH electrodes, respectively, due to the enhanced conductivity and accelerated electron transfer. Notably, the final ZIF-90-based biosensor exhibited a substantial increase in sensitivity, 10.8 and 1.5 times higher than those of the GOx/Conductive gel and LDH/Conductive gel electrodes, respectively (Fig. 3a and 4a, and S18-S19), along with improved acidic and thermal stability (Fig. 3i and j and 4h,i). These improvements stemmed primarily from the protective confinement and high enzyme loading capacity of the ZIF-90 framework. The systematic optimization validated the distinct and complementary roles of each component within the dual-stage stabilization mechanism.

The performance of dual-biosensors array for simultaneous detection of glucose and lactate was firstly examined. It exhibited negligible cross-talk between glucose and lactate sensors, and both the sensitivities of two sensors were the same as those obtained under individual detection conditions (Fig. 5a). Meanwhile, the dual-biosensors array demonstrated its good performance in a complex artificial sweat matrix detection with the relative sensitivity errors of less than 5 % (Fig. S20 and Table S5), confirming its functionality in conditions mimicking inter-user variability. Especially, the sensors for glucose and lactate retained 95 % and 98 % of their initial sensitivity after solar exposure for 10 h, respectively (Fig. 5b–d), outperforming the unoptimized counterpart (Figs. S18b,d, S19b,e, and S21), demonstrating excellent outdoor stability. The wearability and excellent durability of the dual-biosensors array were verified by 1000 bending recovery cycles at bending angles ranging from 60° to 180°, which retained over 85 % of the initial detection sensitivities of two sensors, and met the practical needs of wearable devices (Fig. 5e and f). The demonstrated robustness, outdoor stability, and mechanical durability made the device well-suited for real-time, multi-parameter physiological monitoring in demanding outdoor athletic settings such as marathons and trail cycling.

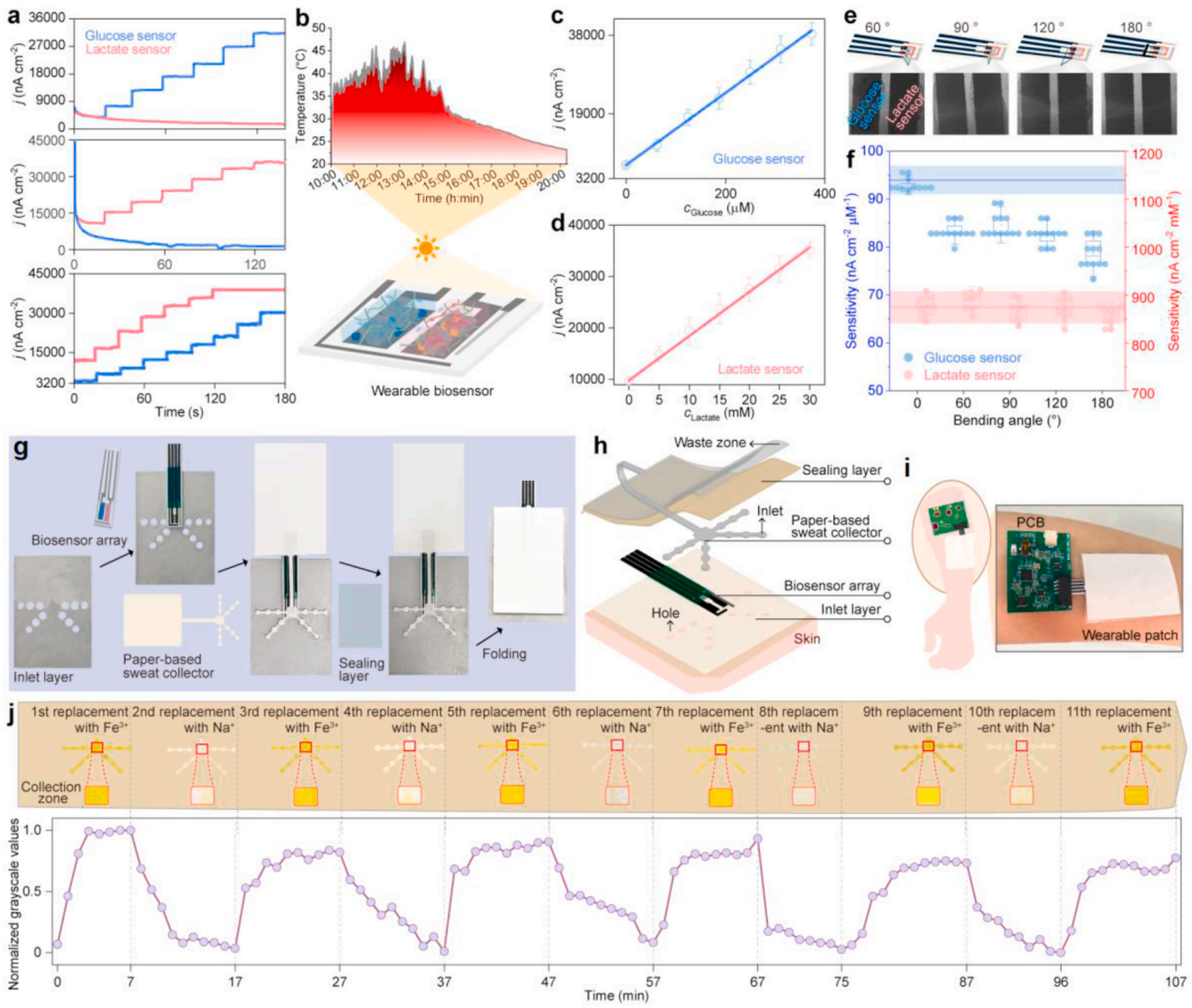


**Fig. 5.** Characterization of wearable biosensing device. (a) Individual and simultaneous amperometric responses of wearable biosensor to varying glucose or/and lactate concentrations. (b) Temperature of biosensor surface upon irradiation of sunlight from 10:00 to 20:00. (c, d) Calibration curves of glucose (c) and lactate (d) sensors after 10 h of sunlight exposure. Data are presented as mean ± SD, $n = 3$. (e, f) Optical images (e) and detection sensitivities (f) of wearable biosensor after 1000 bending/recovery cycles at different bending angles. (g, h) Photographs (g) and schematic (h) for assembly of the wearable patch. (i) Schematic and photograph of the wearable patch interfacing a skin-mounted PCB. (j) Photographs of the collection zone filled with 0.9 M $FeCl_3$ and then 0.1 M NaCl solutions at a rate of 3 μL $cm^{-2}$·$min^{-1}$ and filling time of 10 min for 6 cycles and normalized grayscales of the collection zone at different times.

After assembling the dual-biosensors array and paper-based sweat collector with lnlet and sealing layers (Fig. 5g), the resulting wearable patch could interface with a PCB to form a wearable biosensing device (Fig. 5h), which was designed to be worn on any region of body, such as forearm, for real-time monitoring of sweat glucose and lactate levels (Fig. 5i). Feedstock cost for fabricating a wearable biosensing device, including reticular conductive biogel membranes, SPCE, and paper-based sweat collector, was estimated to be as low as $0.37, demonstrating its potential for affordable daily disposal (Tables S6–S18). The paper-based sweat collector was designed to contain a collection zone of 4 × 4 $mm^2$ matched with the area of biosensors array, which connected to 4 capillary input channels for skin sweat sampling from 12 inlets and 1 outlet channel for waste output (Fig. S22). The diameter and number of inlets and the length and number of input channels were optimized to 2 mm, 3, 9 mm and 4 (Fig. S23–S26). The collection zone could be filled within 15 s (Fig. S27), a result that aligned with the theoretical estimate of ~13 s. This estimate was derived from the collector's design parameters and a sweat rate of 3 μL $cm^{-2}$ $min^{-1}$ (Bariya et al., 2018; Fig. S28 and Supplementary Material 1.9). Furthermore, the collection zone could successively achieve periodic liquid replacement sampling (Fig. 5j).

### 3.6. On-body testing of the wearable biosensing device

The on-body sweat sensing performance of the wearable biosensing device was evaluated by continuous detections of sweat glucose and lactate in 12 volunteers during the running exercise. The wearable device was worn on the forearm of participants, where the sweat samples were periodically collected using centrifuge tubes for synchronous detections of glucose and lactate with colorimetric assay kits (Fig. 6a). The sweat glucose and lactate levels obtained from the device were real-time displayed on a paired smartphone. The readings showed strong correlation with the colorimetric assays, with correlation coefficients of 0.94 and 0.90, respectively (Fig. S29), demonstrating that the device could

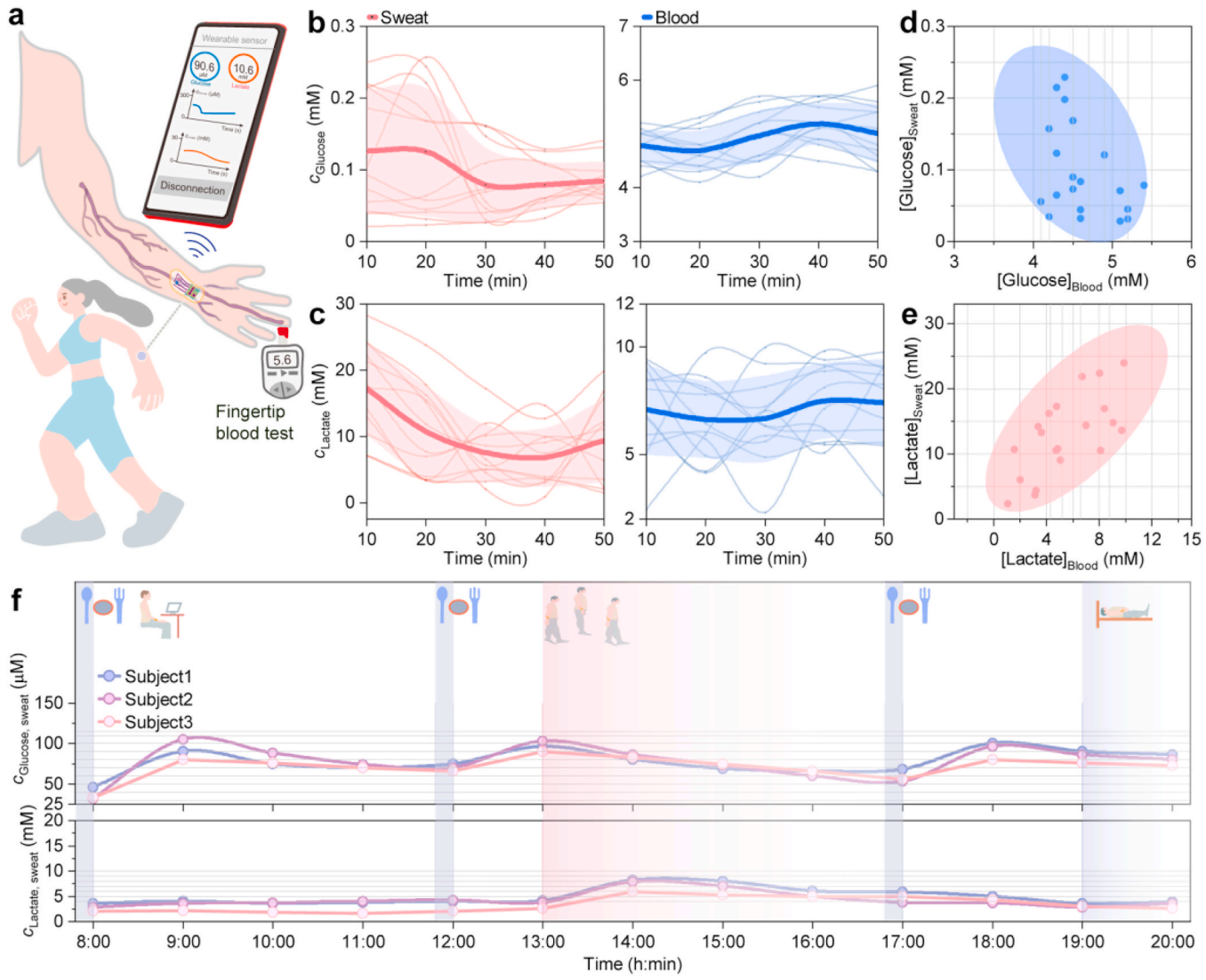


**Fig. 6.** Continuous on-body monitoring of sweat glucose and lactate with wearable biosensing device compared with corresponding fingertip blood test. (a) Illustration of sweat glucose and lactate monitoring during running exercise using a forearm-mounted wearable device. (b, c) Simultaneous detection of sweat and blood glucose (b) and lactate (c) in 12 subjects (6 male and 6 female) during 50-min running. Thick solid lines and shaded bands indicate the mean ± SD. (d, e) Sweat-to-blood concentration correlations for glucose (d) and lactate (e) across all subjects. (f) Continuous sweat glucose and lactate monitoring during 12-h daily activities under thermally induced perspiration.

reliably quantify sweat metabolite levels.

To gain deeper insights into the dynamics of sweat glucose and lactate, parallel blood measurements were conducted during 50-min exercise. The sweat glucose concentration was stable at the beginning of exercise, declined after exercise for 20 min, and slightly rebounded after exercise for 32 min, which lagged the change of blood glucose (Fig. 6b). The latter slightly declined at the beginning of exercise, raised after 20 min, and then slightly declined again at 40 min. The sweat lactate displayed a decreasing trend and rebounded at 40 min, while the blood lactate slightly decreased and raised at 30 min, indicating the similar lag phenomenon of sweat lactate change (Fig. 6c). The overall levels of sweat glucose were 30–110 times lower than blood glucose, while sweat lactate levels were 1.4–2 folds higher than blood lactate, which was consistent with previous report (Yu et al., 2025). The low correlation coefficients among individuals suggested the relatively weak correlations of metabolites due to the complex transport mechanisms (Fig. 6d and e).

The real-life applicability of the wearable device was further evaluated under non-exercise conditions with 3 volunteers. Each volunteer underwent 12 cycles of thermal stimulation using heating pads to sweat (20 min heating followed by a 40-min interval) while carrying out daily activities including food intake, standing and sitting (Fig. 6f). No skin irritation was observed during or after the 12-h monitoring period, indicating a low risk during short-term use (Fig. S30). Both the sweat glucose concentrations showed the similar changes after food intake. In contrast, the sweat lactate concentration remained relatively stable under resting conditions, except the concentration raise during outdoors walking. These preliminary observations were entirely consistent with those reported previously (Ding et al., 2024), highlighting the applicability of wearable biosensing device for daily sweat monitoring.

## 4. Conclusion

We developed a durable, environmentally adaptive wearable biosensor array for continuous sweat glucose and lactate monitoring. Its core is an in-situ formed reticular conductive biogel interface with ZIF-90@enzyme, endowing it with high sensitivity, reproducibility, and stability against pH, temperature, mechanical stress, and solar exposure. After integrating this biosensing array with a paper-based sweat collector, and a wireless PCB, the resulting wearable sweat biosensing

device successfully tracked biomarkers during a variety of daily activities. Future work will focus on optimizing the wearability via rigid-flex electronics and validating the system in larger clinical cohorts, paving the way for robust and practical personalized health monitoring.

## CRediT authorship contribution statement

**Qian Yu:** Writing – original draft, Methodology, Investigation, Formal analysis, Data curation, Conceptualization. **Jun Sun:** Formal analysis. **Chen Yuan:** Validation. **Chao Zhao:** Formal analysis. **Yunlong Chen:** Formal analysis. **Jie Wu:** Writing – review & editing, Supervision, Resources, Methodology, Funding acquisition, Formal analysis. **Siqi Yu:** Investigation. **Hong Liu:** Software, Resources. **Huangxian Ju:** Writing – review & editing, Supervision, Project administration, Methodology, Funding acquisition, Conceptualization.

## Declaration of competing interest

The authors declare that they have no known competing financial interests or personal relationships influencing the work reported in this work.

## Acknowledgements

This work was supported by the National Natural Science Foundation of China (21890741, 21827812, and 21635005) and the Independent Research Foundation from State Key Laboratory of Analytical Chemistry for Life Science (5431ZZXM24010).

## Appendix A. Supplementary data

Supplementary data to this article can be found online at https://doi.org/10.1016/j.bios.2025.118312.

## Data availability

No data was used for the research described in the article.

## References

Arwani, R.T., Tan, S.C.L., Sundarapandi, A., Goh, W.P., Liu, Y., Leong, F.Y., Yang, W., Zheng, X.T., Yu, Y., Jiang, C., Ang, Y.C., Kong, L., Teo, S.L., Chen, P., Su, X., Li, H., Liu, Z., Chen, X., Yang, L., Liu, Y., 2024. https://doi.org/10.1038/s41563-024-01918-9.

Bai, J., Liu, D., Tian, X., Wang, Y., Cui, B., Yang, Y., Dai, S., Lin, W., Zhu, J., Wang, J., Xu, A., Gu, Z., Zhang, S., 2024. Sci. Adv. 10 (16), eadl1856. https://doi.org/10.1126/sciadv.adl1856.

Baik, S., Lee, J., Jeon, E.J., Park, B.Y., Kim, D.W., Song, J.H., Lee, H.J., Han, S.Y., Cho, S. W., Pang, C., 2021. Sci. Adv. 7. https://doi.org/10.1126/sciadv.abf5695 eabf5695.

Bandodkar, A.J., Lee, S.P., Huang, I., Li, W., Wang, S., Su, C.J., Jeang, W.J., Hang, T., Mehta, S., Nyberg, N., Gutruf, P., Choi, J., Koo, J., Reeder, J.T., Tseng, R., Ghaffari, R., Rogers, J.A., 2020. Nat. Electron. 3, 554–562. https://doi.org/10.1038/s41928-020-0443-7.

Bariya, M., Nyein, H.Y.Y., Javey, A., 2018. Nat. Electron. 1, 160–171. https://doi.org/10.1038/s41928-018-0043-y.

Brasier, N., Wang, J., Gao, W., Sempionatto, J.R., Dincer, C., Ates, H.C., Güder, F., Olenik, S., Schauwecker, I., Schaffarczyk, D., Vayena, E., Ritz, N., Weisser, M., Mtenga, S., Ghaffari, R., Rogers, J.A., Goldhahn, J., 2024. Nature 636, 57–68. https://doi.org/10.1038/s41586-024-08249-4.

Chen, Y., Li, G., Mu, W., Gao, J., Wan, X., Lu, D., Wen, D., 2023. Anal. Chem. 95, 3864–3872. https://doi.org/10.1021/acs.analchem.2c05613.

Davis, N., Heikenfeld, J., Milla, C., Javey, A., 2024. Nat. Biotechnol. 42, 860–871. https://doi.org/10.1038/s41587-023-02059-1.

Ding, S., Saha, T., Yin, L., Liu, R., Khan, M.I., Chang, A.-Y., Lee, H., Zhao, H., Liu, Y., Nazemi, A.S., Zhou, J., Chen, C., Li, Z., Zhang, C., Earney, S., Tang, S., Djassemi, O., Chen, X., Lin, M., Sandhu, S.S., Moon, J.-M., Moonla, C., Nandhakumar, P., Park, Y., Mahato, K., Xu, S., Wang, J., 2024. Nat. Electron. 7, 788–799. https://doi.org/10.1038/s41928-024-01236-7.

Dong, K., Peng, X., An, J., Wang, A.C., Luo, J., Sun, B., Wang, J., Wang, Z.L., 2020. Nat. Commun. 11, 2868. https://doi.org/10.1038/s41467-020-16642-6.

Furukawa, H., Cordova, K.E., O'Keeffe, M., Yaghi, O.M., 2013. Science 341, 974. https://doi.org/10.1126/science.1230444.

Gao, W., Emaminejad, S., Nyein, H.Y.Y., Challa, S., Chen, K., Peck, A., Fahad, H.M., Ota, H., Shiraki, H., Kiriya, D., Lien, D.-H., Brooks, G.A., Davis, R.W., Javey, A., 2016. Nature 529, 509–514. https://doi.org/10.1038/nature16521.

Gong, S., Lu, Y., Yin, J., Levin, A., Cheng, W., 2024. Chem. Rev. 124, 455–553. https://doi.org/10.1021/acs.chemrev.3c00502.

Hardy, C., Kociok-Kohn, G., Buchard, A., 2022. Chem. Commun. 58 (36), 5463–5466. https://doi.org/10.1039/d2cc01322c.

Istrate, O.-M., Rotariu, L., Bala, C., 2021. Chemosensors 9, 74. https://doi.org/10.3390/chemosensors9040074.

Jagannath, B., Lin, K.C., Pali, M., Sankhala, D., Muthukumar, S., Prasad, S., 2021. Bioengineering & Transl. Med 6 (3), e10220. https://doi.org/10.1002/btm2.10220.

Kim, S., Lee, B., Reeder, J., Seo, S.H., Lee, S.-U., Hourlier-Fargette, A., Shin, J., Sekine, Y., Jeong, H., Oh, Y.S., Aranyosi, A.J., Lee, S.P., Model, J.B., Lee, G., Seo, M.-H., Kwak, S.S., Jo, S., Park, G., Han, S., Park, I., Jung, H.-I., Ghaffari, R., Koo, J., Braun, P.V., Rogers, J.A., 2020. Proc. Natl. Acad. Sci. U.S.A 117, 27906–27915. https://doi.org/10.1073/pnas.2012700117.

Komkova, M.A., Eliseev, A.A., Poyarkov, A.A., Daboss, E.V., Evdokimov, P.V., Eliseev, A. A., Karyakin, A.A., 2022. Biosens. Bioelectron. 202, 113970. https://doi.org/10.1016/j.bios.2022.113970.

Kumar, N., Lin, Y.-J., Huang, Y.-C., Liao, Y.-T., Lin, S.-P., 2023. Talanta 265, 124888. https://doi.org/10.1016/j.talanta.2023.124888.

Li, C., Zhang, M., Huang, C., 2024. Alex. Eng. J. 105, 218–229. https://doi.org/10.1016/j.aej.2024.06.085.

Li, C.J., Hu, J., Gao, G., Chen, J.H., Wang, C.S., Zhou, H., Chen, G., Qu, P., Lin, P., Zhao, W.W., 2022. Adv. Funct. Mater. 33 (8), 2211277. https://doi.org/10.1002/adfm.202211277.

Liang, K., Ricco, R., Doherty, C.M., Styles, M.J., Bell, S., Kirby, N., Mudie, S., Haylock, D., Hill, A.J., Doonan, C.J., Falcaro, P., 2015. Nat. Commun. 6, 7240. https://doi.org/10.1038/ncomms8240.

Liang, W., Xu, H., Carraro, F., Maddigan, N.K., Li, Q., Bell, S.G., Huang, D.M., Tarzia, A., Solomon, M.B., Amenitsch, H., Vaccari, L., Sumby, C.J., Falcaro, P., Doonan, C.J., 2019. J. Am. Chem. Soc. 141, 2348–2355. https://doi.org/10.1021/jacs.8b10302.

Lin, Y.J., Bariya, M., Javey, A., 2021. Adv. Funct. Mater. 31, 2008087. https://doi.org/10.1002/adfm.202008087.

Madhvapathy, S.R., Cho, S., Gessaroli, E., Forte, E., Xiong, Y., Gallon, L., Rogers, J.A., 2025. Nat. Rev. Nephrol. 21, 443–463. https://doi.org/10.1038/s41581-025-00961-2.

Min, J., Demchyshyn, S., Sempionatto, J.R., Song, Y., Hailegnaw, B., Xu, C., Yang, Y., Solomon, S., Putz, C., Lehner, L.E., Schwarz, J.F., Schwarzinger, C., Scharber, M.C., Sani, E.S., Kaltenbrunner, M., Gao, W., 2023. Nat. Electron. 6, 630–641. https://doi.org/10.1038/s41928-023-00996-y.

Mohan, B., Virender, Gupta, R.K., Pombeiro, A.J.L., Solovev, A.A., Singh, G., 2024. Adv. Funct. Mater. 34, 2405231. https://doi.org/10.1002/adfm.202405231.

Parlak, O., Keene, S.T., Marais, A., Curto, V.F., Salleo, A., 2018. Sci. Adv. 4. https://doi.org/10.1126/sciadv.aar2904 eaar2904.

Petroody, S.S.A., Hashemi, S.H., Skrlep, L., Music, B., van Gestel, C.A.M., Skapin, A.S., 2023. Polymers 15 (21), 4322. https://doi.org/10.3390/polym15214322.

Ray, T.R., Ivanovic, M., Curtis, P.M., Franklin, D., Guventurk, K., Jeang, W.J., Chafetz, J., Gaertner, H., Young, G., Rebollo, S., Model, J.B., Lee, S.P., Ciraldo, J., Reeder, J.T., Hourlier-Fargette, A., Bandodkar, A.J., Choi, J., Aranyosi, A.J., Ghaffari, R., McColley, S.A., Haymond, S., Rogers, J.A., 2021. Sci. Transl. Med.e 13. https://doi.org/10.1126/scitranslmed.abd8109 eabd8109.

Rwei, A.Y., Lu, W., Wu, C.S., Human, K., Suen, E., Franklin, D., Fabiani, M., Gratton, G., Xie, Z.Q., Deng, Y.J., Kwak, S.S., Li, L.Z., Gu, C., Liu, A., Rand, C.M., Stewart, T.M., Huang, Y.G., Weese-Mayer, D.E., Rogers, J.A., 2020. Proc. Natl. Acad. Sci. U.S.A 117, 31674–31684. https://doi.org/10.1073/pnas.2019786117.

Saha, T., Songkakul, T., Knisely, C.T., Yokus, M.A., Daniele, M.A., Dickey, M.D., Bozkurt, A., Velev, O.D., 2022. ACS Sens. 7, 2037–2048. https://doi.org/10.1021/acssensors.2c00830.

Schuck, A., Kim, H.E., Moreira, J.K., Lora, P.S., Kim, Y.-S., 2021. Sensors 21, 1852. https://doi.org/10.3390/s21051852.

Semperger, O.V., Osvath, Z., Pasztor, S., Suplicz, A., 2022. Polym. Eng. Sci. 62 (6), 2079–2088. https://doi.org/10.1002/pen.25990.

Sempionatto, J.R., Lasalde-Ramírez, J.A., Mahato, K., Wang, J., Gao, W., 2022. Nat. Rev. Chem 6, 899–915. https://doi.org/10.1038/s41570-022-00439-w.

Shieh, F.-K., Wang, S.-C., Yen, C.-I., Wu, C.-C., Dutta, S., Chou, L.-Y., Morabito, J.V., Hu, P., Hsu, M.-H., Wu, K.C.W., Tsung, C.-K., 2015. J. Am. Chem. Soc. 137, 4276–4279. https://doi.org/10.1021/ja513058h.

Su, T., Mi, Z., Xia, Y., Jin, D., Xu, Q., Hu, X., Shu, Y., 2023. Talanta 260, 124620. https://doi.org/10.1016/j.talanta.2023.124620.

Sun, J., Chu, R., Wu, X., Yu, Q., Xiao, W., Ao, H., Wang, Y., Wu, T., Ju, H., Wu, J., Lei, J., 2025. J. Am. Chem. Soc. 147, 17936–17945. https://doi.org/10.1021/jacs.5c02949.

Thapa, M., Sung, R., Heo, Y.S., 2021. Biosensors (Basel) 11, 507. https://doi.org/10.3390/bios11120507.

Torrente-Rodriguez, R.M., Tu, J., Yang, Y., Min, J., Wang, M., Song, Y., Yu, Y., Xu, C., Ye, C., IsHak, W.W., Gao, W., 2020. Matter 2, 921–937. https://doi.org/10.1016/j.matt.2020.01.021.

Wang, M., Ye, C., Yang, Y., Mukasa, D., Wang, C., Xu, C., Min, J., Solomon, S.A., Tu, J., Shen, G., Tang, S., Hsiai, T.K., Li, Z., McCune, J.S., Gao, W., 2025. Nat. Mater. 24, 589–598. https://doi.org/10.1038/s41563-024-02096-4.

Wang, M., Yang, Y., Min, J., Song, Y., Tu, J., Mukasa, D., Ye, C., Xu, C., Heflin, N., McCune, J.S., Hsiai, T.K., Li, Z., Gao, W., 2022. Nat. Biomed. Eng. 6, 1225–1235. https://doi.org/10.1038/s41551-022-00916-z.

Weng, X., Li, M., Chen, L., Peng, B., Jiang, H., 2024. Talanta 279, 126675. https://doi.org/10.1016/j.talanta.2024.126675.

Wu, Z.-Q., Cao, X.-Q., Hua, Y., Yu, C.-M., 2024. Anal. Chem. 96, 3087–3095. https://doi.org/10.1021/acs.analchem.3c05216.
Xu, Y., De la Paz, E., Paul, A., Mahato, K., Sempionatto, J.R., Tostado, N., Lee, M., Hota, G., Lin, M., Uppal, A., Chen, W., Dua, S., Yin, L., Wuerstle, B.L., Deiss, S., Mercier, P., Xu, S., Wang, J., Cauwenberghs, G., 2023. Nat. Biomed. Eng. 7, 1307–1320. https://doi.org/10.1038/s41551-023-01095-1.
Xuan, X., Chen, C., Molinero-Fernandez, A., Ekelund, E., Cardinale, D., Swarén, M., Wedholm, L., Cuartero, M., Crespo, G.A., 2023. ACS Sens. 8, 2401–2409. https://doi.org/10.1021/acssensors.3c00708.
Yang, D.S., Ghaffari, R., Rogers, J.A., 2023. Science 379, 760–761. https://doi.org/10.1126/science.abq5916.
Yang, X., Yi, J., Wang, T., Feng, Y., Wang, J., Yu, J., Zhang, F., Jiang, Z., Lv, Z., Li, H., Huang, T., Si, D., Wang, X., Cao, R., Chen, X., 2022. Adv. Mater. 34 (44), 2201768. https://doi.org/10.1002/adma.202201768.
Yang, Y., Song, Y., Bo, X., Min, J., Pak, O.S., Zhu, L., Wang, M., Tu, J., Kogan, A., Zhang, H., Hsiai, T.K., Li, Z., Gao, W., 2020. Nat. Biotechnol. 38, 217–224. https://doi.org/10.1038/s41587-019-0321-x.
Yao, M.S., Lv, X.J., Fu, Z.H., Li, W.H., Deng, W.H., Wu, G.D., Xu, G., 2017. Angew. Chem. Int. Ed. 56 (52), 16510–16514. https://doi.org/10.1002/anie.201709558.
Yin, J., Wang, S., Tat, T., Chen, J., 2024. Nat. Rev. Bioeng. 2, 541–558. https://doi.org/10.1038/s44222-024-00175-4.
Yin, L., Cao, M., Kim, K.N., Lin, M., Moon, J.-M., Sempionatto, J.R., Yu, J., Liu, R., Wicker, C., Trifonov, A., Zhang, F., Hu, H., Moreto, J.R., Go, J., Xu, S., Wang, J., 2022. Nat. Electron. 5, 694–705. https://doi.org/10.1038/s41928-022-00843-6.
Yu, Q., Wu, J., Xiao, W.C., Zhao, C., Zhang, W.Q., Chen, Y.L., Liu, Y., Liu, H., Zhou, J., Ding, L., Ju, H.X., 2025. Cell Rep. Phys. Sci. 6, 102389. https://doi.org/10.1016/j.xcrp.2024.102389.